JTTEE5 20:351–357
DOI: 10.1007/s11666-010-9538-4
1059-9630/$19.00 © ASM International

Peer Reviewed

Characteristics of Cu Film Deposited Using VLPPS

N. Zhang, F. Sun, L. Zhu, C. Verdy, M.P. Planche, H. Liao, C. Dong, and C. Coddet

(Submitted May 4, 2010; in revised form June 29, 2010)

Cu coatings were obtained by the very low pressure plasma spray (VLPPS) process using a torch F4-VB. The tank pressure was varied from 1 to 5 mbar: these specific conditions can be allowed to obtain a higher vapor condensation fraction in the coating. Different sizes of powders are used to compare the vaporization level. The other possible influencing factors for obtaining compact film-like coating are also considered such as the distance between the torch and substrate, the orientation of the vapors and also the substrate temperatures. Microstructures of coatings are analyzed and combined with the results of plasma diagnostics. Jobin-Yvon spectrometer (type TRIAX190, UK) and Plasus Specline Spectroscopy software are both used for detecting and analyzing plasma spectrum data. The value of plasma electronic excited temperature T_e was calculated through choosing H_α and H_β two atom spectra. The results showed that the plasma belongs to cold plasma in the local thermodynamic equilibrium situation in VLPPS.

Keywords VLPPS, Cu, Film, Spectral diagnostic, Electronic temperature

1. Introduction

The very low pressure plasma spray (VLPPS) process has been developed with the aim of depositing uniform and thin coatings with large area coverage by plasma spraying. This can be used in applications where large areas cannot be covered by the PVD process or require expensive processing costs, and where traditional thermal spray coatings have reached their limits based on porosity and thickness requirements (Ref 1-4). For example, in atmospheric plasma spraying (APS), the problems which usually occur are multi-imperfections such as easily oxidized and relatively low adhesive strength for thick coatings (Ref 5). A lot of work on the research and application of LPPS have been carried out with ceramic materials (Ref 4, 6-10). Nowadays, this type of research has also been combined with optical emission spectroscopy (OES) analyses.

The variation of the operating pressure is the most influencing factor on the characteristics of the plasma jet (length, diameter velocity, density, and viscosity) which have an impact on the spray particle conditions. In this article, the operated pressure ranges from 1 to 10 mbar, which benefits the evaporating particles and results in a film-like coating. Cu coating was produced for initial investigations using this new technology. The plasma jet with Cu powder is shown in Fig. 1. Plasma diagnostics were carried out by OES to further understand the properties of plasma jet in VLPPS.

2. Experimental

Experiments were performed using a Sulzer MetcoF4-VB gun, which was mounted on a 6-axis robot manipulator (ABB, IRB 1400) inside the vacuum chamber. Argon was also used as the carrier gas for the feedstock injection. Spray process parameters are shown in Table 1.

During the spray process, evaporation and sublimation processes occur whereby individual atoms are released from the surface of a liquid or solid body, respectively, by thermal energy. Optical emission spectrometry was used to study the different species in the vapor phase and to characterize the plasma jet properties (Ref 11-16). The OES of the plasma jet was measured using a Jobin-Yvon spectrometer (type TRIAX190, UK) equipped with CCD detector. The installation of detection equipment is shown in Fig. 2. The sensor head was mounted on a specially designed tube with a front optical window to allow measurements inside the vacuum chamber. This tube was equipped with a water cooling unit to protect the sensor head from the heat flux coming from the plasma jet. Before using the spectrometer, calibration was carried out.

This article is an invited paper selected from presentations at the 2010 International Thermal Spray Conference and has been expanded from the original presentation. It is simultaneously published in *Thermal Spray: Global Solutions for Future Applications, Proceedings of the 2010 International Thermal Spray Conference*, Singapore, May 3-5, 2010, Basil R. Marple, Arvind Agarwal, Margaret M. Hyland, Yuk-Chiu Lau, Chang-Jiu Li, Rogerio S. Lima, and Ghislain Montavon, Ed., ASM International, Materials Park, OH, 2011.

N. Zhang, Key Laboratory of Materials Modification, Dalian University of Technology, 116085 Dalian, China and LERMPS-UTBM Site de Sévenans, 90010 Belfort Cedex, France; **F. Sun, L. Zhu, C. Verdy, M.P. Planche, H. Liao,** and **C. Coddet**, LERMPS-UTBM Site de Sévenans, 90010 Belfort Cedex, France; and **C. Dong**, Key Laboratory of Materials Modification, Dalian University of Technology, 116085 Dalian, China. Contact e-mail: Nannan.Zhang@utbm.fr.

Keeping the distance between the optical axis and the torch exit constant and moving the torch with a constant speed, different species were recorded in the perpendicular direction of plasma jet profiles. For data acquisition, a grating of 1200 grooves/mm was selected and the spectral region was varied from 100 to 1000 nm which includes Cu and Ar/H_2 spectra with a focal length of 190 mm for each mirror. The spectral analysis software was applied for detecting and analyzing the spectral data.

Fig. 1 VLPPS plasma jet using F4-VB torch injected Cu powders at 1 mbar

Table 1 Spray process parameters

Powder	Cu
Pressure, mbar	1, 5
Size of particle, µm	14-64
Voltage of plasma, V	52
Current of plasma, A	700
Amount of the feed powder, g/min	10
Argon flow, l/min	40
Hydrogen flow, l/min	8
Spraying distance, cm	40, 47

The coatings were deposited on stainless steel plates, which were grit-blasted with alumina prior to spraying. The polished cross section and fractured section of the plasma sprayed coatings were analyzed using scanning electron (JSM5800LV, JEOL, Japan) and optical microscopy (Nikon, Japan).

2.1 Effect of Particle Size Analyzed by OES

Concerning the effect of powder, three sizes of powder were used at 5 mbar pressure; these were <20 µm, 20-40 µm, and 40-64 µm. The size distributions of Cu powders were measured by Mastersizer2000 (MALVERN Instruments, UK). Figure 3 indicates that the three kinds of powders show a near Gaussian size distribution with a mean particle size of 17.966, 33.764, and 58.365 µm.

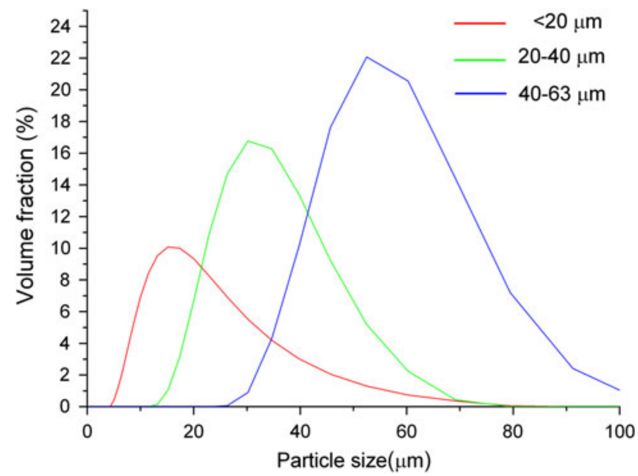

Fig. 3 Size distributions of the used Cu powders

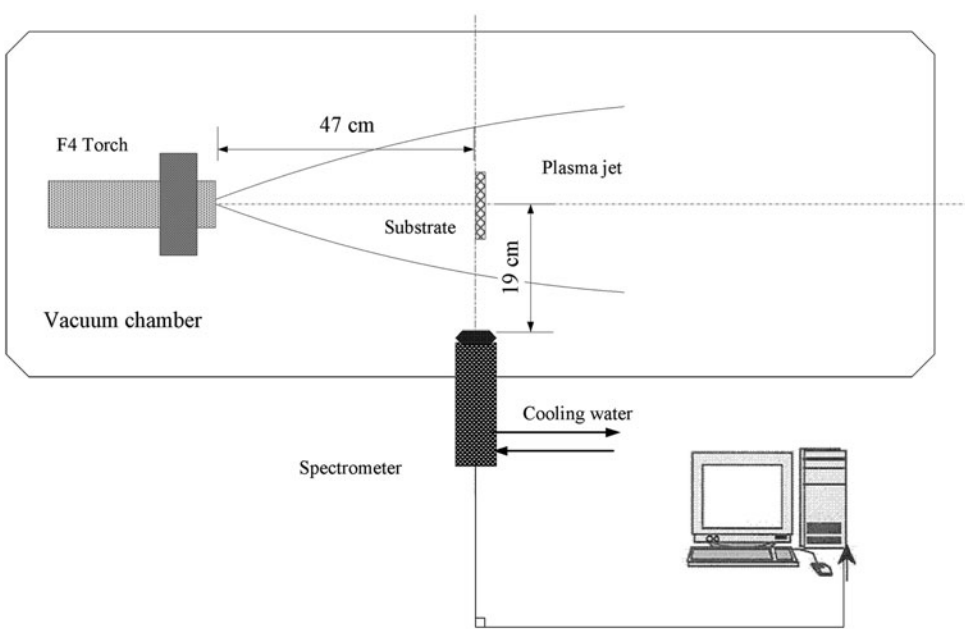

Fig. 2 Schematic diagram of the OES diagnostics system

To examine the effect of powder size, OES was used to verify the degree of evaporation. OES is the spectral analysis of light emission from the plasma and probably the most widely used method for the diagnosis of plasma processes (Ref 17, 18). By measuring the wavelengths and intensities of the emitted spectral lines, one can identify the neutral particles and ions present in the plasma. Figure 4(a) shows the spectrum of the plasma jet without powder, whereas Fig. 3(d) and 4(b, c) correspond to plasma and Cu signals. The comparison of the Cu signals show that Cu lines at 521.4 nm are present with injected powder size less than 20 µm. According to the Atomic & Molecular spectral database, the finer powder is fit to be evaporated in this case. In the following experiments, only the powder of <20 µm particle fraction was used at different pressures for improved evaporation. Furthermore, the effect of powder feed rate on powder volatilization should also be considered. From our experience, it was found that an excessively high powder feed rate could decrease the evaporation of copper particles (Ref 19).

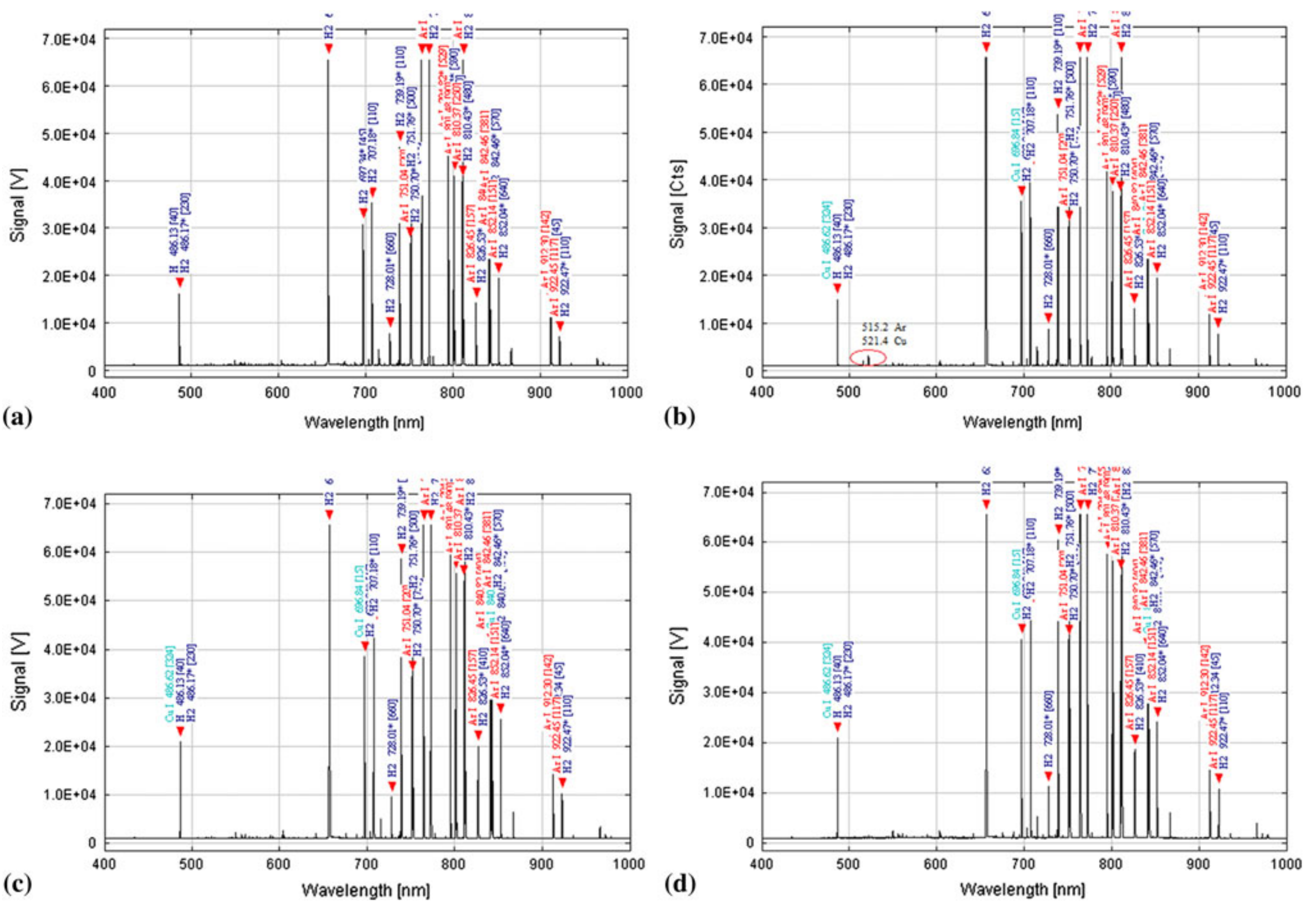

Fig. 4 Optical spectrum of the plasma jet (Ar/H_2) at 5 mbar: (a) Without powders, (b) injected Cu powders <20 µm, (c) injected Cu powders 20-40 µm and (d) injected Cu powders 40-64 µm

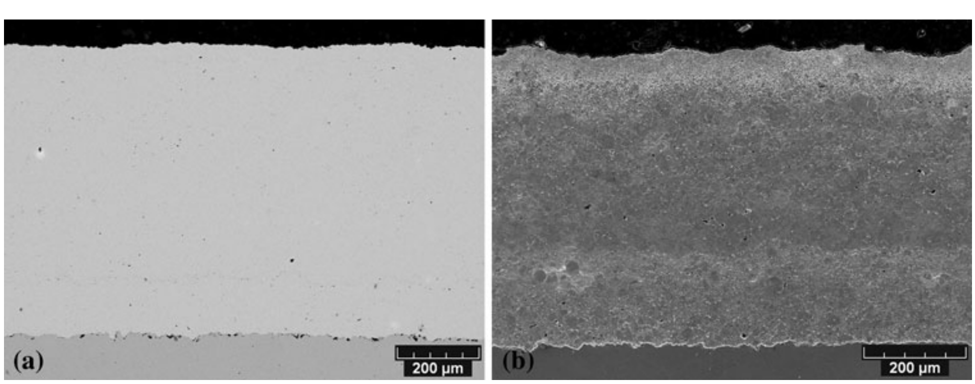

Fig. 5 Cu coating using different parameters by VLPPS: (a) dense coating and (b) etched coating

2.2 Effect of Spray Distance and Injected Gas

With different gas parameters and spray distances, typical plasma sprayed Cu coatings by VLPPS are shown in Fig. 5(a). The pressure was constant at 1 mbar.

After etching the polished coating using a solution of $FeCl_3$, the effect of operating parameters on the coating structure was clearly shown in Fig. 5(b), two boundaries were clearly identified. The coating near to the substrate was prepared with Ar and H_2 gas and the spray distance was kept 40 cm. The middle region of coating was produced at the 47 cm spray distance. For the upper region of coating the distance returned to 40 cm without injecting H_2 gas. Larger grains about 5 μm were present close to the substrate, which was caused by the influence of higher enthalpy due to H_2 injection. The high substrate temperature makes the metal grains grow rapidly. The similar research has been done by Refke et al., who make use of this high temperature for the formation of a well-defined YSZ columnar microstructure (Ref 20).

Unlike the typical structures of the plasma sprayed coating, there are fewer pores but also some unmelted particles in the coating. Figure 6 shows these fine grains in the upper region. As the plasma enthalpy decreased, the temperature for nucleation became low, these fine grains appeared. This shows that it is possible to obtain nanocrystals by controlling spray parameters such as substrate temperature, powder size, powder feed rate, spray distance, and specific mixture of plasma gases.

2.3 Characterization of Cu Film-Like Coatings

It was determined that the stainless steel substrate is be easily melted when the spray plume was impacting it for a long time. In order to avoid substrate overheating from the high enthalpy of the plasma, the coating was obtained by producing a fast relative motion between the plasma jet and the substrate. To investigate the effect of surface roughness, glass substrates were used. Because of their lower melting point, the substrates were placed a little further away in order to be kept away from the plasma plume.

Figure 7 shows the spectra of the plasma jet without powder (Fig. 7a) and injected Cu powder (Fig. 7b). The spectral Cu lines correspond to the Atomic & Molecular spectral database and the intensity of spectral Cu lines is so high that it indicates the injected material could be well vaporized.

The cross section of Cu coating is shown in Fig. 8. Some small particles are observed near to the surface which can

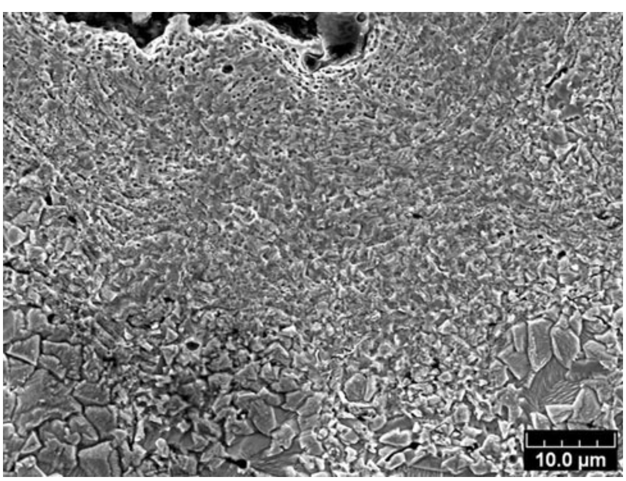

Fig. 6 Microstructure obtained in the upper region of the coating

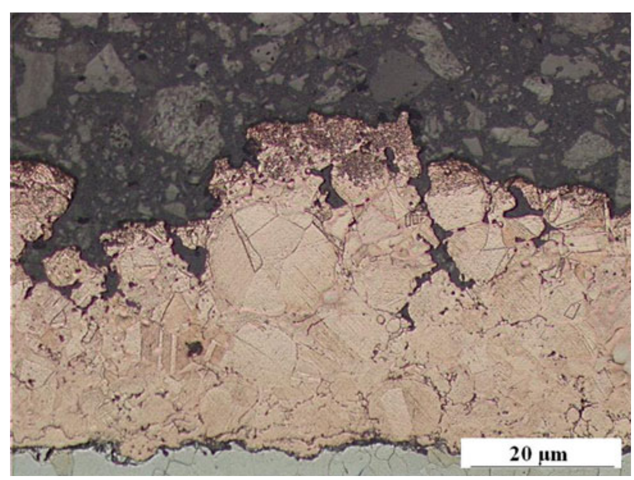

Fig. 8 Typical etched fractured section of Cu coating

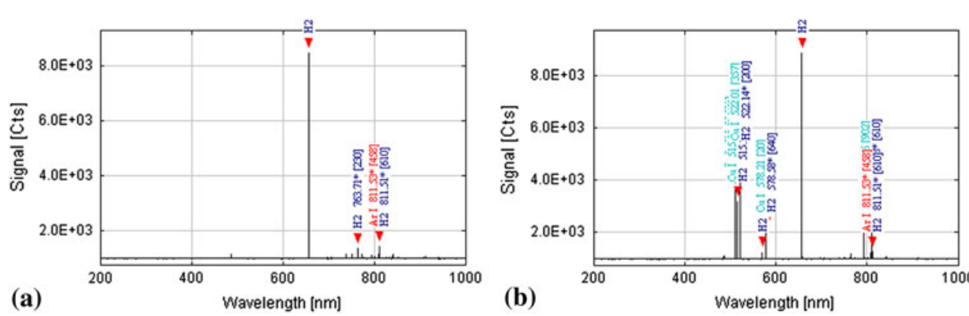

Fig. 7 Optical spectrum of the plasma jet (Ar/H_2) at 1 mbar: (a) without powders and (b) injected Cu powder

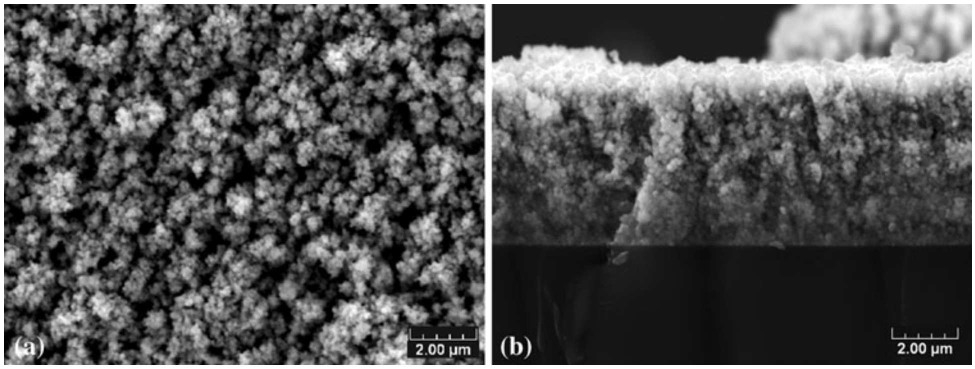

Fig. 9 Cu film-like deposited at the glass substrate by VLPPS: (a) surface of the coating and (b) grain growing at the gap of coating

be easily eroded. They were formed in the cooling process after spraying stopped. Finally, it is difficult to obtain nanocrystals directly by the typical method owing to the excessive heating of the substrate.

Figure 9(a) shows very fine particles produced by Cu vapor on the surface of the glass substrate. The Cu coating is thin and dense as compared to traditional thin films grown by PVD technology (Fig. 9b). The coating is about 5-µm thick and the growth direction can be seen.

2.4 Calculation of Plasma Electron Temperature

As the hydrogen spectral lines are in the visible region of the spectrum and easy to identify, it is generally used for this type of plasma diagnosis and investigation. In this work, the detection distance was fixed at 47 cm, the current intensity is 700 A, and the feeding of H_2 plasma gas was kept at 4 L/min with Ar gas 40 L/min. The relative intensity of spectral lines is shown in Fig. 10.

As measuring the spectral relative intensity is easier than measuring the absolute intensity, the relative intensity measurement is widely used to get the plasma electron temperature T_e (Ref 21). Then, plasma electron temperature can be determined based on the relative intensity of the two spectral lines of the same atom. For low electron density plasmas, the steady-state coronal model is applied. Radiative decay is equal to electron impact excitation and electron temperature determines the population of the excited states under the assumption that the electron velocity distribution is Maxwell distribution and the population of the excited states follows the Boltzmann distribution. Therefore, the line intensity ratio is assumed to depend solely on the electron temperature in low pressure plasma (Ref 22). Based on this method the electron temperature is reasonably accurate even for low density plasma, which is shown in the following expression:

$$\frac{n_m}{n_n} = \frac{g_m}{g_n} \exp\left[-\frac{E(m) - E(n)}{kT_e}\right] \quad \text{(Eq 1)}$$

Here, n, g, k, and E are, respectively, the particle density, the statistical weight, the Boltzmann constant, and the energy of upper level of emission spectral line. In the plasma radiation spectrum, spectral intensity is expressed as follows:

$$I_{mr} = n_m A_{mr} h\nu_{mr} \quad \text{(Eq 2)}$$

A, h, and ν are the transition probability, Planck constant, and electronic spontaneous transition frequency, respectively. r presents the lower transition energy level which can be as the same energy level.

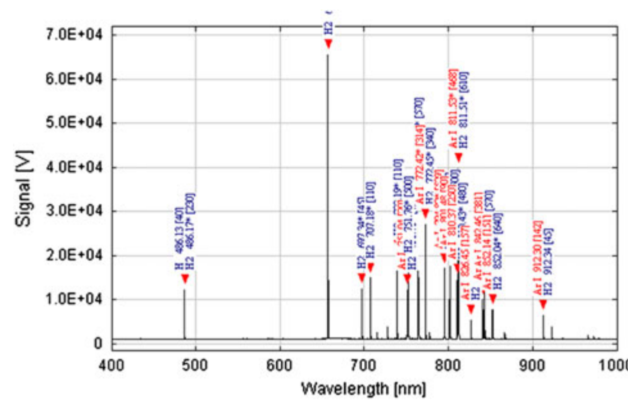

Fig. 10 Ar/H_2 spectral emission lines

In order to improve the calculation accuracy and reduce the calculation quantity, it is important to choose the spectrum under the same energy level. By eliminating r, the final formula of the electron temperature is:

$$T_e = -\frac{E_n - E_m}{k}\left[\ln\left(\frac{A_n g_n I_m \lambda_m}{A_m g_m I_n \lambda_n}\right)\right]^{-1} \quad \text{(Eq 3)}$$

The results obtained are summarized in Table 2.

Strictly, in the condition of local thermal equilibrium, the electron temperature is different from the temperature in the part of the local thermal equilibrium condition. When the electron temperature ranged from 4000 to 64,000 K, electron excitation can be approximately considered to be local thermal equilibrium. The use of this formula gives the plasma electron temperature should be accurately referred to as electronic excitation temperature or excitation temperature (Ref 23). At this point, electron

Table 2 The calculation results

Spectrum	H_α	H_β
λ, nm	486.416	656.723
I, a.u	12318	65535
ν, s^{-1}	4.5651×10^{14}	6.1635×10^{14}
g	32	16
Energy level	4-2	3-2

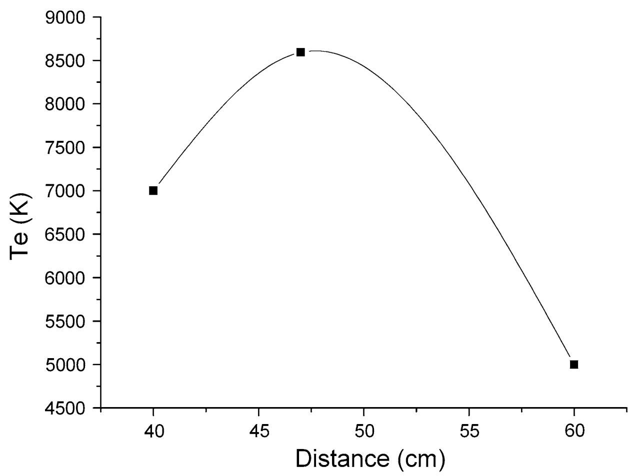

Fig. 11 The calculated value of T_e in different detection distance

and ion or neutral particle collision process is almost no loss of energy, so that $T_e \gg T_i$ and T_n. The electron temperature through the formula is 8592 K which belongs to the region of cold plasma ($T_e < 10^4$ K). Jin et al. (Ref 16) chose the third spectrum H_γ to calculate the plasma electron temperature and found that there were obvious differences among the results calculated from every two spectra at the same discharge current. Except the influence of measured error from the spectrum system, the relative value of spectral intensity has an effect on the temperature:

$$\frac{\Delta T_e}{T_e} = \frac{kT_e}{|E_n - E_m|} \frac{\Delta(I_m/I_n)}{I_m/I_n} \quad \text{(Eq 4)}$$

That is to say, the more the difference of the relative spectral intensity between H_α and H_β, the higher the value of ΔT_e. Hence, it can be considered that through the changes of spectrum intensity to get the trends of electronic temperature in order to research the plasma characteristics in the low pressure plasma spray. For example, in this work the detection distances were 40 and 60 cm. The H_α spectrum intensity decreased from 7000 to 5000 whereas H_β spectrum intensity was kept at 65,535. The corresponding plasma electron temperatures were 5261 and 4274 K. It may be the reason that this condition belong to the part of local thermal equilibrium system and the population of these excited state atoms does not absolutely follow the Boltzmann distribution. The graph of the electron temperature versus different detection distances is shown in Fig. 11.The high T_e temperature may be due to the detection position of the sensor placed just at the Mach cone of plasma plume.

From previous works (Ref 24, 25) that the electron temperature in the low pressure plasma jets is fairly low (0.3-0.7 eV), it is found according with this experiment, which through the conversion of Boltzmann constant (Ref 26), the electron temperature is about 0.37-0.74 eV.

3. Conclusions

Using the VLPPS process with a F4-VB torch, a Cu film-like dense coating was successfully deposited. With a powder fraction of <20 μm, the particles can be better evaporated although there were a few particles or lamellae structure in the coating, but nanocrystal particles were produced by Cu vapor on the surface of the glass substrate. For obtaining nanocrystals the sizes of powder, substrate temperature, and roughness seem to be critical parameters. For studying the characters of plasma plume, the electron temperature was calculated in this work which ranges from 0.37 to 0.74 eV in the situation of local thermal equilibrium. This research will be continued in the future.

References

1. E.J. Young, E. Mateeva, J.J. Moore, B. Mishra, and M. Loch, Low Pressure Plasma Spray Coatings, *Thin Solid Films*, 2000, **377-378**, p 788-792
2. Z. Salhi, S. Guessasma, P. Gougeon, D. Klein, and C. Coddet, Diagnostic of YSZ In-Flight Particle Characteristics under Low Pressure VPS conditions, *Aerospace Sci. Technol.*, 2005, **9**, p 203-209
3. J.L. Dorier, M. Gindrat, C. Hollenstein, M. Loch, A. Refke, A. Salito, and G. Barbezat, Plasma Jet Properties in a New Spraying Process at Low Pressure for Large Area Thin Film Deposition, International Thermal Spray 2001, Singapore, 28-30 May
4. J. Disam, K. Luebbers, U. Neudert, and A. Sickinger, Effect of LPPS Spray Parameters on the Structure of Ceramic Coatings, *J. Therm. Spray Technol.*, 1994, **3**, p 142-147
5. W. Ma, W.X. Pan, and C.K. Wu, Preliminary Investigations on Low-pressure Laminar Plasma Spray Processing, *Surf. Coat. Technol.*, 2005, **191**, p 166-174
6. H. Huang, K. Eguchi, M. Kambara, and T. Yoshida, Ultrafast Thermal Plasma Physical Vapor Deposition of Yttria-Stabilized Zirconia for Novel Thermal Barrier Coatings, *J. Therm. Spray Technol.*, 2006, **15**, p 83-91
7. C.H. Chang and E. Pfender, Heat and Momentum Transport to Particulates Injected into Low-pressure (~80 mbar) Nonequilibrium Plasma, *IEEE Trans. Plasma Sci.*, 1990, **18**, p 958-967
8. K.H. Baik, P.S. Grant, and B. Cantor, The Equiaxed-banded Microstructural Transition During Low Pressure Plasma Spraying, *Acta Mater.*, 1994, **52**, p 199-208
9. S. Sodeoka, M. Suzuki, and K. Ueno, Effects of High-Pressure Plasma Spraying for Yttria-Stabilized Zirconia Coating, *J. Therm. Spray Technol.*, 1996, **5**, p 277-282
10. D. Matejka and B. Benko, *Plasma Spraying of Metallic and Ceramic Materials*, Wiley, NY, 1989, p 12
11. H. Hamatani, W.S. Crawford, and M.A. Cappelli, Optical Measurements of Plasma Velocity and Temperature in a Low-rate, Low-power LPPS System, *Surf. Coat. Technol.*, 2002, **162**, p 79-92

12. M. Gindrat, A. Refke, and R. Schmid, Process Characterization of LPPS Thin Film Processes with Optical Diagnostics, Thermal Spray 2007: Global Coating Solutions May 14-16 2007, p 826-831
13. S. Iordanova and I. Koleva, Optical Emission Spectroscopy Diagnostics of Inductively-Driven Plasmas in Argon Gas at Low Pressures, *Spectrochim. Acta B*, 2007, **62**, p 344-356
14. J. Blain, L. Pouliot, F. Nadeau, M. Lamontagne, and C. Moreau, Optimization of Sensor Optics for Industrial Thermal Spray Sensors, Thermal Spray 2007: Global Coating Solutions, May 14-16, 2007, p 832-836
15. R. L. Boxman, P. J. Martin, and D. M. Sanders, Handbook of Vacuum Arc Science and Technology, Noyes publications, 1995, p 21
16. D.Z. Jin, Z.H. Yang, P.Y. Tang, K.X. Xiao, and J.Y. Dai, Hydrogen Plasma Diagnosis in Penning Ion Source by Optical Emission Spectroscopy, *Vacuum*, 2009, **83**, p 451-453
17. A. Grill, Cold Plasma in Materials Fabrication, Wiley-IEEE Press, New York, 1994, p 138
18. L.A. Garcia, E. Restrepo, H. Jiménez, H.A. Castillo, R. Ospina, V. Benavides, and A. Devia, Diagnostics of Pulsed Vacuum Arc Discharges by Optical Emission Spectroscopy and Electrostatic Double-probe Measurements, *Vacuum*, 2006, **81**, p 411-416
19. Z. Salhi, D. Klein, P. Gougeon, and C. Coddet, Development of Coating by Thermal Plasma Spraying under Very Low-pressure Condition <1 mbar, *Vacuum*, 2005, **77**, p 145-150
20. A. Refke, M. Gindrat, K. von Niessen, and R. Damani, LPPS Thin Film: A Hybrid Coating Technology between Thermal Spray and PVD for Functional Thin Coatings and Large Area Applications, Thermal Spray 2007: Global Coating Solutions, May 14-16, 2007, p 705-710
21. S. Semenov and B. Cetegen, Spectroscopic Temperature Measurements in Direct Current Arc Plasma Jets Used in Thermal Spray Processing of Materials, *J. Therm. Spray Technol.*, 2001, **10**, p 326-336
22. J.H. Cui, Z.F. Xu, J.L. Zhang, Q.Y. Nie, G.H. Xu, and L.L. Ren, Online Diagnosis of $CH_4 + H_2$ Discharge Spectrum for Plasma Electronic Excitation Temperature at Atmosphere, Science of China, 2008, vol 38, p 1053-1057
23. Z.Y. Guo and W.H. Zhao, *Arc and Thermal Plasma*, Science Press, Beijing, 1986, p 268
24. J.J. Beulens, C. Gastineau, N. Guerrassimov, J. Koulidiati, and D.C. Schram, Atomic and Molecular Emission Spectroscopy on an Expanding Argon/methane Plasma, *Plasma Chem. Plasma Process.*, 1994, **14**, p 15-42
25. M. Gindrat, J.L. Dorier, C. Hollenstein, A. Refke, and G. Barbezat, Characterization of Supersonic Low Pressure Plasma Jets with Electrostatic Probes, *Plasma Sour. Sci. Technol.*, 2004, **13**, p 484-492
26. B. Widom, *Statistical Mechanics: A Concise Introduction for Chemists*, Cambridge University Press, Cambridge, 2002, p 2